J|A|C|S
ARTICLES
Published on Web 03/01/2003

Redoxable Nanosheet Crystallites of MnO_2 Derived via Delamination of a Layered Manganese Oxide

Yoshitomo Omomo, Takayoshi Sasaki,*,† Lianzhou Wang, and Mamoru Watanabe

Contribution from the Advanced Materials Laboratory, National Institute for Materials Science, 1-1 Namiki, Tsukuba, Ibaraki 305-0044, Japan, and CREST, Japan Science and Technology Corporation (JST)

Received November 19, 2002; E-mail: sasaki.takayoshi@nims.go.jp

Abstract: This paper reports on the swelling and exfoliation behavior of a layered protonic manganese oxide, $H_{0.13}MnO_2 \cdot 0.7H_2O$, in a solution of tetrabutylammonium (TBA) hydroxide and the formation and characterizations of unilamellar two-dimensional crystallites of MnO_2. At low doses of TBA ions, layered manganese oxide was observed to undergo normal intercalation, yielding a TBA intercalated phase with a gallery height of 1.25 nm. With a large excess of TBA ions, osmotic swelling occurred, giving rise to a very large intersheet separation of 3.5−7 nm. In an intermediate TBA concentration range, the sample exhibited a broad X-ray diffraction profile with superimposed diffraction features due to intercalation and osmotic swelling. The component responsible for the broad profile was isolated by centrifuging the mixture twice at different speeds, and the recovered colloid was identified as a pile of MnO_2 nanosheets, corresponding to the individual host layer of the precursor layered manganese oxide. Observations by transmission electron microscopy and atomic force microscopy revealed high two-dimensional anisotropy with a lateral dimension of submicrometers and a thickness of ~0.8 nm. The nanosheet exhibited broad optical absorption with a peak at 374 nm ($\epsilon = 1.13 \times 10^4$ mol^{-1} dm^3 cm^{-1}). The restacking process of the colloidal MnO_2 nanosheets was followed by aging the colloid at a relative humidity of 95%. The broad diffraction pattern due to the exfoliated sheets weakened with time and eventually resolved into two sharp distinct profiles attributable to a TBA intercalation compound with an intersheet spacing of 1.72 nm and an osmotically swollen hydrate with >10 nm at a very early stage. As drying progressed, the former phase became more abundant without a change in interlayer distance, while the degree of swelling of the latter phase gradually decreased to 2.7 nm that remained unchanged on further aging. Subsequent drying at a lower humidity collapsed the 2.7 nm phase. The resulting single 1.72 nm phase was dehydrated by heating at 150 °C to produce a phase with a contracted interlayer spacing of 1.3 nm.

Introduction

Nanometer-scale materials often exhibit intriguing physical and chemical properties that are rarely present in bulk materials. A wide variety of nanotubes and nanoparticles have been investigated extensively in the past decade.[1,2]

Recently, nanosheets have been synthesized as a new class of nanoscale materials by disintegrating a layered compound into the constituent single layers.[3] These unilamellar crystallites have a thickness on the order of nanometers or smaller, with lateral dimensions of submicro- to micrometers. This extremely high anisotropy and a thickness of molecular dimensions are strikingly different from nanoparticles which generally have a spherical shape. In addition, nanosheets are characterized by novel aspects such as the single-crystal quality, high crystallinity, well-defined composition, and colloidal and polyeletrolytic nature as well as new or enhanced physicochemical properties. Layered materials exfoliated to date include clay minerals,[4] layered transition metal oxides,[5−7] chalcogenides,[8] phosphates,[9] graphite oxide,[10] and layered double hydroxides,[11] providing wide selections of nanosheet crystallites. The features above

† CREST, Japan Science and Technology Corporation (JST).

(1) *Encyclopedia of Nanoscience and Nanotechnology*; Nalwa, H. S., Ed.; American Scientific Publishers: Stevenson Ranch, CA, 2003.
(2) *Nanoparticles and Nanostructured Films*; Fendler, J. H., Ed.; Wiley-VCH: Weinheim, Germany, 1998.
(3) (a) Jacobson, A. J. *Mater. Sci. Forum* **1994**, *152*−*153*, 1−12. (b) Jacobson, A. J. *Comprehensive Supramolecular Chemistry*; Alberti, G., Bein, T., Eds.; Elsevier Science: Oxford, U.K., 1996; Vol. 7, pp 315−335.
(4) (a) MacEwan, D. M. C.; Wilson, M. J. In *Crystal Structures of Clay Minerals and Their X-ray Identification*; Brindley, G. W., Brown, G., Eds.; Mineralogical Society: London, 1980. (b) Nadeau, P. H.; Wilson, M. J.; McHardy, W. J.; Tait, J. M. *Science* **1984**, *225*, 923−925. (c) Nadeau, P. H.; Wilson, M. J.; McHardy, W. J.; Tait, J. M. *Clay Miner.* **1984**, *19*, 67−76. (d) Nadeau, P. H.; Wilson, M. J.; McHardy, W. J.; Tait, J. M. *Clay Miner.* **1984**, *19*, 757−769. (e) Tamura, K.; Sasaki, T.; Yamada, H.; Nakazawa, H. *Langmuir* **1999**, *15*, 5509−5512.
(5) (a) Sasaki, T.; Watanabe, M.; Hashizume, H.; Yamada, H.; Nakazawa, H. *J. Chem. Soc., Chem. Commun.* **1996**, 229−230. (b) Sasaki, T.; Watanabe, M.; Hashizume, H.; Yamada, H.; Nakazawa, H. *J. Am. Chem. Soc.* **1996**, *118*, 8329−8335. (c) Sasaki, T.; Watanabe, M. *J. Am. Chem. Soc.* **1998**, *120*, 4682−4689. (d) Harada, M.; Sasaki, T.; Ebina, Y.; Watanabe, M. *J. Photochem. Photobiol., A* **2002**, *148*, 273−276.
(6) (a) Treacy, M. M. J.; Rice, S. B.; Jacobson, A. J.; Lewandowski, J. T. *Chem. Mater.* **1990**, *2*, 279−286. (b) Domen, K.; Ebina, Y.; Ikeda, S.; Tanaka, A.; Kondo, J. N.; Maruya, K. *Catal. Today* **1996**, *28*, 264−274. (c) Schaak, R. E.; Mallouk, T. E. *Chem. Mater.* **2000**, *12*, 3427−3434. (d) Schaak, R. E.; Mallouk, T. E. *Chem. Mater.* **2002**, *14*, 1455−1471. (e) Han, Y.-S.; Park, I.; Choy, J.-H. *J. Mater. Chem.* **2001**, *11*, 1277−1282. (f) Ebina, Y.; Sasaki, T.; Watanabe, M. *Solid State Ionics* **2002**, *151*, 177−182.
(7) Saupe, G. B.; Waraksa, C. C.; Kim, H.-N.; Han, Y. J.; Kaschak, D. M.; Skinner, D. M.; Mallouk, T. E. *Chem. Mater.* **2000**, *12*, 1556−1562.

10.1021/ja021364p CCC: $25.00

can invite a range of applications, particularly in the field of nanoscience and nanomaterials. One of the highlights is the fabrication of nanocomposites of organic polymer/inorganic host materials, which exhibit useful properties such as high mechanical strength.[12] Furthermore, the shape control of particulates as thin flakes and hollow spheres has been achieved through freeze- or spray-drying techniques.[13]

Among the various nanosheet materials, nanosheets derived from functional layered materials are particularly interesting and important. Mallouk et al. have carried out an extensive study on the exfoliation of various types of layered niobates and related materials. They reported the formation of nanosheets in perovskite-related architecture, typically $Ca_2Nb_3O_{10}$,[6c,d] and scrolls or tubulars of Nb_6O_{17} nanosheets.[7] We have demonstrated that titanium oxide, one of the most useful oxides, can be obtained in nanosheet form by delaminating layered titanates into the constituent single sheets.[5] These niobate and titania nanosheets are expected to be useful for photochemical and photocatalytic applications owing to their semiconducting nature.

Due to their colloidal and polyelectrolytic nature, nanosheets can be self-assembled layer-by-layer to construct larger nanostructured systems. Several groups have demonstrated that the Langmuir−Brodgett procedure and electrostatic self-assembly via sequential adsorption are effective for this purpose.[14−18] The layer-by-layer assembly of various nanoscale materials and functional molecules may allow us to tailor "superlattices" or "supramolecular systems", through which one can design complex functions that cannot be achieved using a single material. One example is a nanoassembly of acceptors and donors intervened by zirconium phosphate nanosheets which attains effective charge separation.[19]

The development of a wide range of nanoscale materials with various properties is very important in the design of nanodevices with sophisticated functionality. However, most nanosheets synthesized to date are semiconducting or insulating materials. The range of applications of nanoassemblies could therefore be widened significantly if nanosheet materials with new physical and chemical properties can be developed. A material class with promising features is the series of layered ternary oxides with the general formula AMO_2 where A and M represent alkali metals (Li, Na, K) and transition metals (Mn, Co, Ni, Fe), respectively.[20] A typical composition is $LiCoO_2$, which is used as a cathode material in commercial Li ion batteries.[21] Delamination of these materials will afford nanomaterials with a feasible redox capability. A range of applications, including energy storage and new solar cells, may be realized by combining these materials with semiconducting nanosheets.

Very recently, two groups have studied the swelling behavior of birnessite-type layered manganese oxide upon reaction with large amines and ammonium ions.[22] Liu et al. found that birnessite intercalated with quaternary ammonium ions lost basal diffraction lines when washed with water, suggesting delamination, and Gao et al. reported that nanometer-sized manganese oxides were formed in the intercalation process. However, the swelling behaviors reported by these groups are not completely consistent. Furthermore, occurrence of exfoliation into single layers, which is one of the most important points, has not been demonstrated persuasively.

The present study is undertaken to derive manganese oxide nanosheets with redoxable capability. Swelling and delamination reactions of a layered manganese oxide $H_{0.13}MnO_2 \cdot 0.7H_2O$ are examined in detail because a deep understanding of the reactions is essential to obtain unilamellar nanosheets. The obtained unilamellar crystallites were characterized in terms of optical absorption properties and morphology.

Results and Discussion

Starting Layered Manganese Oxides. The layered manganese oxide $K_{0.45}MnO_2$ gave X-ray diffraction (XRD) data which can be indexed as a rhombohedral system (*R*3*m*). The refined cell parameters ($a = 0.2879(2)$ nm, $c = 1.907(1)$ nm) are in good agreement with the reported data.[23] Interlayer K ions were extracted by repeated acid treatments. The degrees of K ion removal were 92.2%, 96.9%, and 98.2% by reaction for 3, 7, and 10 days, respectively. The sample prepared by acid treatments for 10 days was employed for equilibration studies of swelling and delamination behavior. With a mean Mn valence of 3.87, as determined by titration, the composition

(8) (a) Murphy, D. W.; Hull, G. W., Jr. *J. Chem. Phys.* **1975**, *62*, 973−978. (b) Lerf, A.; Schöllhorn, R. *Inorg. Chem.* **1977**, *16*, 2950−2956. (c) Joensen, P.; Frindt, R. F.; Morrison, S. R. *Mater. Res. Bull.* **1986**, *21*, 457−461. (d) Yang, D.; Jiménez Sandoval, S.; Divigalpitiya, W. M. R.; Irwin, J. C.; Frindt, R. F. *Phys. Rev. B* **1991**, *43*, 12053−12056. (e) Yang, D.; Frindt, R. F. *J. Phys. Chem. Solids* **1996**, *57*, 1113−1116.
(9) (a) Alberti, G.; Casciola, M.; Costantino, U. *J. Colloid Interface Sci.* **1985**, *107*, 256−263. (b) Alberti, G.; Dionigi, C.; Giontella, E.; Murcia-Mascaros, S. *J. Colloid Interface Sci.* **1997**, *188*, 27−31. (c) Alberti, G.; Giontella, E.; Murcia-Mascarós, S. *Inorg. Chem.* **1997**, *36*, 2844−2849. (d) Alberti, G.; Cavalaglio, S.; Dionigi, C.; Marmottini, F. *Langmuir* **2000**, *16*, 7663−7668. (e) Yamamoto, N.; Okuhara, T.; Nakato, T. *J. Mater. Chem.* **2001**, *11*, 1858−1863.
(10) (a) Kovtyukhova, N. I.; Ollivier, P. J.; Martin, B. R.; Mallouk, T. E.; Chizhik, S. A.; Buzaneva, E. V.; Gorchinskiy, A. D. *Chem. Mater.* **1999**, *11*, 771−778. (b) Kotov, N. A.; Dékány, I.; Fendler, J. H. *Adv. Mater.* **1996**, *8*, 637. (c) Cassagneau, T.; Fendler, J. H. *Adv. Mater.* **1998**, *10*, 877−881.
(11) (a) Adachi-Pagano, M.; Forano, C.; Besse, J.-P. *Chem. Commun.* **2000**, 91−92. (b) Leroux, F.; Adachi-Pagano, M.; Intissar, M.; Chauviére, S.; Forano, C.; Besse, J.-P. *J. Mater. Chem.* **2001**, *11*, 105−112. (c) Hibino, T.; Jones, W. *J. Mater. Chem.* **2001**, *11*, 1321−1323.
(12) (a) Krishnamoorti, R.; Vaia, R. A.; Giannelis, E. P. *Chem. Mater.* **1996**, *8*, 1728−1734. (b) Lerner, M. M.; Oriakhi, C. O. Polymers in Ordered Nanocomposites. In *Handbook of Nanophase Materials*; Goldstein, A. N., Ed.; The Marcel Dekker: New York, 1997; pp 199−219.
(13) (a) Sasaki, T.; Nakano, S.; Yamauchi, S.; Watanabe, M. *Chem. Mater.* **1997**, *9*, 602−608. (b) Iida, M.; Sasaki, T.; Watanabe, M. *Chem. Mater.* **1998**, *10*, 3780−3782.
(14) Yamaki, T.; Asai, K. *Langmuir* **2001**, *17*, 2564−2567.
(15) (a) Okamoto, K.; Tamura, K.; Taniguchi, M.; Yamagishi, A. *Colloid Surf., A* **1999**, *169*, 241. (b) Umemura, Y.; Yamagishi, A.; Schoonheydt, R.; Persoons, A.; Schryver, D. F. *J. Am. Chem. Soc.* **2002**, *124*, 992−997.
(16) (a) Kleinfield, E. R.; Ferguson, G. S. *Science* **1994**, *265*, 370−373. (b) Kleinfield, E. R.; Ferguson, G. S. *Chem. Mater.* **1995**, *7*, 2327−2331. (c) Lvov, Y.; Ariga, K.; Ichinose, I.; Kunitake, T. *Langmuir* **1996**, *12*, 3038−3044. (d) Kotov, N. A.; Haraszti, T.; Turi, L.; Zavala, G.; Geer, R. E.; Dékány, I.; Fendler, J. H. *J. Am. Chem. Soc.* **1997**, *119*, 6821−6832. (e) Kim, D. W.; Blumstein, A.; Kumar, J.; Tripathy, S. K. *Chem. Mater.* **2001**, *13*, 1916−1922.
(17) (a) Keller, S. W.; Kim, H.-N.; Mallouk, T. E. *J. Am. Chem. Soc.* **1994**, *116*, 8817−8818. (b) Kim, H.-N.; Keller, S. W.; Mallouk, T. E.; Schmitt, J.; Decher, G. *Chem. Mater.* **1997**, *9*, 1414−1421. (c) Fang, M.; Kim, C. H.; Saupe, G. B.; Kim, H.-N.; Waraksa, C. C.; Miwa, T.; Fujishima, A.; Mallouk, T. E. *Chem. Mater.* **1999**, *11*, 1526−1532. (d) Schaak, R. E.; Mallouk, T. E. *Chem. Mater.* **2000**, *12*, 2513−2516.
(18) (a) Sasaki, T.; Ebina, Y.; Watanabe, M.; Decher, G. *Chem. Commun.* **2000**, 2163-2164. (b) Sasaki, T.; Ebina, Y.; Tanaka, T.; Harada, M.; Watanabe, M.; Decher, G. *Chem. Mater.* **2001**, *13*, 4661−4667. (c) Sasaki, T.; Ebina, Y.; Fukuda, K.; Tanaka, T.; Harada, M.; Watanabe, M. *Chem. Mater.* **2002**, *14*, 3524−3530.
(19) Keller, S. W.; Johnson, S. A.; Brigham, E. S.; Yonemoto, E. H.; Mallouk, T. E. *J. Am. Chem. Soc.* **1995**, *117*, 12879−12880.
(20) (a) Delmas, P. C.; Fouassier, C.; Hagenmuller, P. *Inorg. Synth.* **1983**, *22*, 55−61. (b) Ohzuku, T.; Ueda, A. *Solid State Ionics* **1994**, *69*, 201−211.
(21) Tarascon, J.-M.; Armand, M. *Nature* **2001**, *414*, 359−367.
(22) (a) Liu, Z.-H.; Ooi, K.; Kanoh, H.; Tang, W.-P.; Tomida, T. *Langmuir* **2000**, *16*, 4154−4164. (b) Gao, Q.; Giraldo, O.; Tong, W.; Suib, S. L. *Chem. Mater.* **2001**, *13*, 778−786.
(23) Delmas, P. C.; Fouassier, C. *Z. Anorg. Allg. Chem.* **1976**, *420*, 184−192.

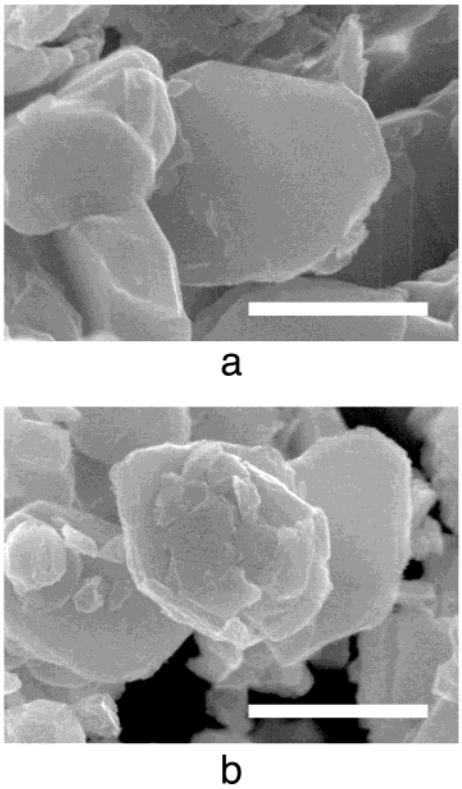

Figure 1. Scanning electron micrographs for (a) $K_{0.45}MnO_2$ and (b) $H_{0.13}MnO_2 \cdot 0.7H_2O$. Scale bar represents 1 μm.

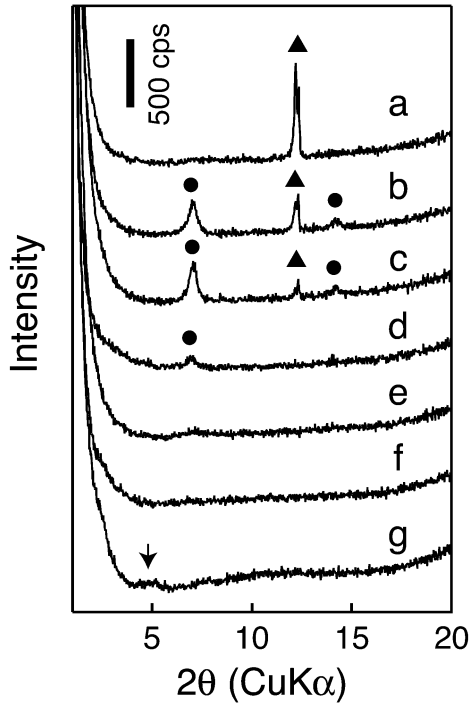

Figure 2. XRD patterns for a mixture of a layered manganese oxide, $H_{0.13}MnO_2 \cdot 0.7H_2O$, and an aqueous solution of TBAOH. The molar ratios of TBA ions over exchangeable protons in the manganese oxide, TBA^+/H^+, are (a) 0.1, (b) 0.3, (c) 1, (d) 5, (e) 25, (f) 50, and (g) 100. Triangles and circles denote the basal reflections from $H_{0.13}MnO_2 \cdot 0.7H_2O$ (0.73 nm) and the TBA intercalated phase (1.25 nm), respectively, whereas numerals in parentheses indicate the interlayer distance. An arrow indicates a faint diffraction feature, suggesting the formation of a highly swollen phase.

of the product acid-treated for 10 days can be formulated as $H_{0.13}MnO_2 \cdot 0.7H_2O$. These results indicate that K ions were removed via two reaction routes: ion exchange and redox deintercalation involving disproportionation of Mn^{3+} to Mn^{2+} and Mn^{4+}, as has been demonstrated for various types of manganese oxides.[24] The acid-digested sample was highly crystalline, exhibiting a layered structure with a basal distance of 0.73 nm. The structural and compositional data are comparable to those reported for birnessite.[24,25] The samples were composed of platelike crystals with a lateral dimension of submicro- to micrometers (Figure 1).

Swelling Behavior. The swelling behavior of $H_{0.13}MnO_2 \cdot 0.7H_2O$ was examined through treatment with an aqueous solution of tetrabutylammonium hydroxide (abbreviated as TBAOH) at various concentrations. The mixtures exhibited various appearances after vigorous shaking for 10 days. Samples with a low TBA dose ($TBA^+/H^+ \leq 2$) separated into a solid at the bottom of the flask and a clear supernatant solution when shaking was stopped, whereas samples interacted with a larger amount of TBAOH remained colloidal. Although some sedimentation was observed even for these higher-dose samples, the supernatant solution remained dark brown as characteristic of manganese oxides.

Figure 2 shows XRD data of the mixtures. The agitated sample solution was pipetted onto an XRD sample holder and measured at a constant relative humidity of 95%. A large halo was observed at $2\theta = 15-50°$ for all samples (rising portion of the baseline as seen in Figure 2), attributable to X-ray scattering by aqueous water. Also, some samples exhibited sharp diffraction features attributable to the manganese oxide. At $TBA^+/H^+ \leq 1$, there were two noticeable basal series with spacings of 0.73 and 1.25 nm. The former is due to $H_{0.13}MnO_2 \cdot 0.7H_2O$, and the latter may be assigned to a TBA intercalated structure. This was present as the sole phase in the samples with TBA^+/H^+ of 1−25. The peak intensity of this phase decreased with increasing TBA dose to finally disappear at $TBA^+/H^+ = 50$, where the water halo was only observable. A faint diffraction feature (indicated by arrows in Figure) was again discerned at a higher TBA content, implying the presence of a highly swollen phase.

The mixture was then centrifuged at 20 000 rpm for 30 min, and the recovered solid was examined by XRD. The data quality was improved by eliminating the water halo and increasing the content of manganese oxide in the sample. Care was taken to prevent the sample from drying out by conducting measurements at a relative humidity of 95%. The obtained typical data are summarized in Figures 3 and 4. The data for samples at low TBA doses are consistent with those obtained for the aqueous samples. With higher resolution, higher-order basal reflections can be seen. The starting material (0.73 nm) changed into the 1.25 nm phase with increasing TBA dose, which can be understood as a normal intercalation process via phase separation. A slight intersheet shrinkage of 0.01 nm was observed for the former phase at the initial stage, probably due to a change in the hydration state. Similar phenomena have been observed for birnessite layered manganese oxides.[22b,26]

(24) Feng, Q.; Kanoh, H.; Ooi, K. *J. Mater. Chem.* **1999**, *9*, 319−333.
(25) Post, J. E.; Veblen, D. R. *Am. Mineral.* **1990**, *75*, 477−489.
(26) Abou-El-Sherbini, K. S.; Askar, M. H.; Schöllhorn, R. *Solid State Ionics* **2002**, *150*, 407−415.

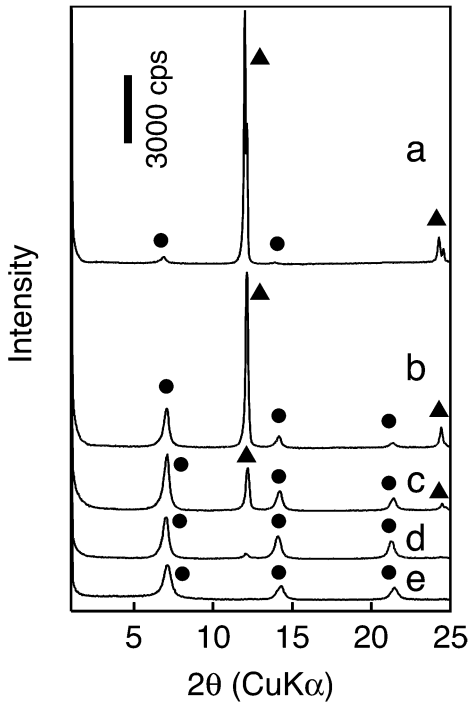

Figure 3. XRD patterns for a solid centrifuged from an aqueous mixture of $H_{0.13}MnO_2 \cdot 0.7H_2O$ and TBAOH. The molar ratios of TBA^+/H^+ are (a) 0.1, (b) 0.3, (c) 0.5, (d) 1, and (e) 2. Triangles and circles denote the basal reflections from $H_{0.13}MnO_2 \cdot 0.7H_2O$ (0.73 nm) and the TBA intercalated phase (1.25 nm), respectively.

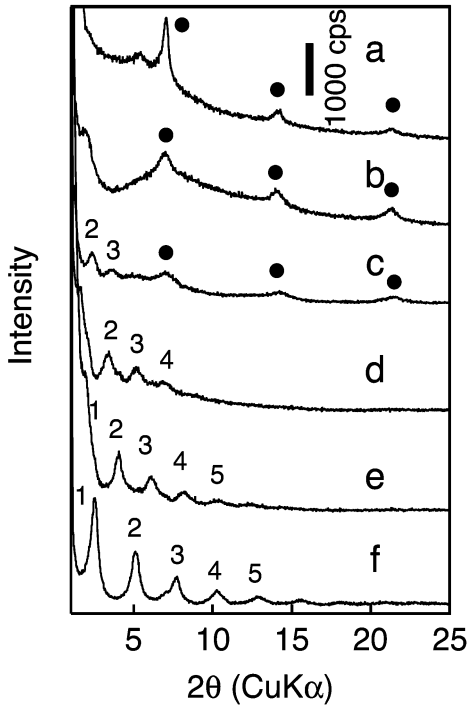

Figure 4. XRD patterns for a colloidal aggregate centrifuged from an aqueous mixture of $H_{0.13}MnO_2 \cdot 0.7H_2O$ and TBAOH. The molar ratios of TBA^+/H^+ are (a) 5, (b) 10, (c) 25, (d) 50, (e) 70, and (f) 100. Numerals next to the peaks represent the order of basal reflections attributable to osmotic swelling. Circles denote the basal reflection from the TBA intercalated phase (1.25 nm).

More detailed information was obtained for samples with $TBA^+/H^+ \geq 5$ (see Figure 4), when compared with the data from aqueous suspensions. The peak assigned to the 1.25 nm phase weakened with increasing TBA dose, disappearing at $TBA^+/H^+ = 50$ and being replaced with a series of diffraction peaks indicative of a very high degree of swelling. These diffraction features were most clearly seen in the sample with $TBA^+/H^+ = 100$. The basal series extended up to eighth orders, suggesting a highly crystalline form with an intersheet separation of 3.5 nm. The peak positions were in agreement with the diffraction features faintly perceptible in the same sample in aqueous form (prior to centrifugation), which indicates that the degree of swelling was preserved after centrifugation.

Similar basal diffraction peaks were observed for the samples with $TBA^+/H^+ < 100$, where the peaks shifted to lower angles with decreasing TBA concentration, indicating that the degree of swelling was enhanced. The intersheet separations were estimated to be 7.2, 5.4, 4.6, and 3.5 nm for the samples with $TBA^+/H^+ = 25$, 50, 70, and 100, respectively. The large intersheet expansion is ascribed to osmotic swelling, where a large volume of the electrolyte solution is introduced into the interlayer space of a layered host. This differs from the ordinary intercalation reaction. Note that the intersheet separation in this range cannot result from the simple accommodation of TBA ions with an estimated size of 0.84−1.05 nm.[17b,22b,27] In osmotic swelling, electric double layers are formed on both sides of the negatively charged nanosheets and charge neutrality of the total system is attained with electrolytes in the double layers. This qualitatively explains the swelling behavior observed in this study; the larger intersheet expansion with decreasing TBA concentration is attributable to a larger volume of TBA solution needed for compensation of the MnO_2 layer charge. This phenomenon is interesting in that reports on high degrees of swelling via osmotic hydration are limited to smectite clay minerals[4] and layered titanates.[5c,d]

Apart from the conspicuous diffraction features due to osmotic swelling and intercalation, there was a broad component most clearly observed at $TBA^+/H^+ = 5$ and 10. This is an important feature because it can be taken as evidence of exfoliation into individual MnO_2 sheets. The interpretation will be described in the following section.

A summary of the XRD results for a system of $H_{0.13}MnO_2 \cdot 0.7H_2O$/TBAOH is shown as a reaction diagram in Figure 5. The layered manganese oxide undergoes normal intercalation at a lower TBA dose, while osmotic swelling is predominant at high TBA concentration and exfoliation into single MnO_2 sheets is promoted at intermediate TBA doses. The ranges in which these reactions predominate overlap with each other. This reaction scheme is similar to that for a layered titanate except for the range of TBA contents in which the reactions predominantly proceed.[5c,d] The close similarity of the reaction diagrams for the two layered materials, manganese oxide and titanate, suggests that this reaction scheme may be valid for other hosts. The difference in stoichiometry for each reaction may be attributable to differences in acid−base properties and the layer charge of these two hosts.

To understand the meaning of the threshold stoichiometry, the solid phase formed at $TBA^+/H^+ = 2$ was recovered by centrifugation, washed, and subsequently air-dried. The chemical composition of the product was identified as $[(C_4H_9)_4N]_{0.11}H_{0.03}MnO_2 \cdot 0.2H_2O$ (Calcd: Mn, 46.9%; C, 18.0%; H, 3.8%; N,

(27) Sasaki, T.; Watanabe, M. *Mol. Cryst. Liq. Cryst. Sci. Technol., Sect. A* **1998**, *311*, 417−422.

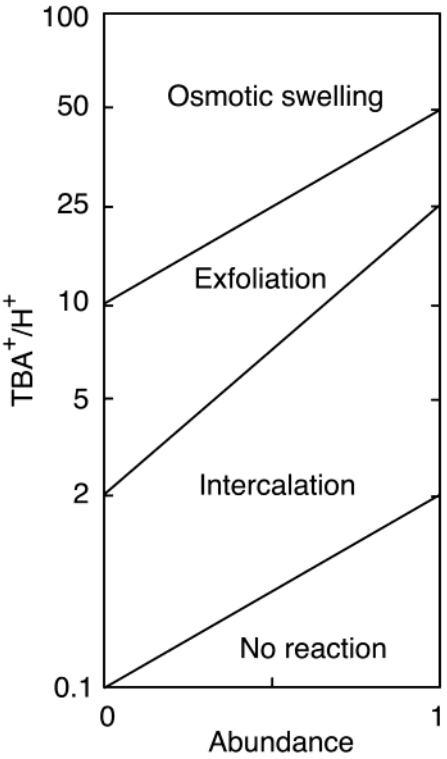

Figure 5. Reaction diagram for a system of $H_{0.13}MnO_2 \cdot 0.7H_2O$ and TBAOH solution.

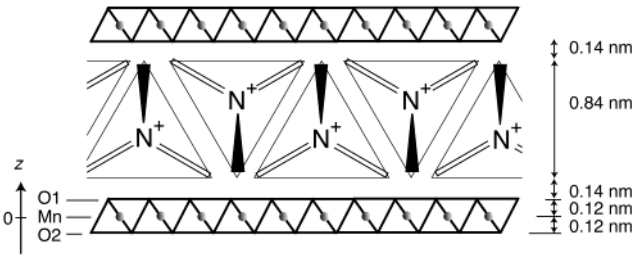

Figure 6. Structure model for the TBA intercalated phase.

1.3%. Found: Mn, 46.7%; C, 18.2%; H, 3.7%; N, 1.3%). The mean oxidation state was 3.86, indicating that TBA ions were introduced into the MnO_2 gallery via ion-exchange. The observed interlayer distance of 1.25 nm may be explained by the accommodation of TBA ions with the C_2 axis aligned along the layer normal, being close to a sum of this TBA dimension in this orientation (0.84 nm)[27,28] and the layer thickness (0.52 nm) (Figure 6).[29] The slight discrepancy may suggest that TBA ions are not perfectly tetrahedral but are somewhat distorted, which may be due to a conformational change in long alkyl chains. If we assume that TBA ions in prefect tetrahedral configuration are close-packed in two dimensions, the packing density would be 0.35 nm^2.[27] Since the unit area for the two-dimensional hexagonal cell of the MnO_2 nanosheets is 0.078 nm^2 ($= 0.3 \times 0.3 \times \sqrt{3}/2$), the theoretical stoichiometry of TBA/MnO_2 for this model is 0.22. If distortion of the TBA ions is taken into account, the packing density becomes lower and, in fact, may approach the observed value. This means that the

(28) The perpendicular orientation of the C_3 axis with respect to the MnO_2 sheet is unlikely because the TBA ionic size in this direction is larger (0.95 nm).
(29) Refer to the layer architecture in Figure 6. If the radius of an oxygen atom is 0.14 nm,[34] the layer thickness is 0.52 nm.

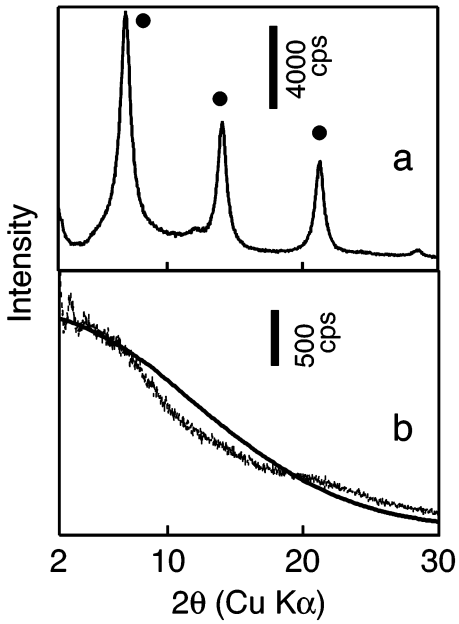

Figure 7. XRD data for a solid phase separated by centrifugation. (a) A sample recovered at a centrifuging speed of 6000 rpm. Circles denote the basal reflections of the 1.25 nm phase. (b) A colloid obtained by centrifugation at 20 000 rpm from the resulting suspension after centrifugation at 6000 rpm. Dotted and solid lines represent the observed profile and the square of the structure factor of the MnO_2 sheet, respectively.

MnO_2 gallery is almost fully packed (close-packed) with TBA ions. Uptake of TBA ions beyond this stoichiometry would inevitably result in large intersheet expansion, which may facilitate high degrees of hydration and conversion into the colloidal state.

Isolation of Colloidal MnO_2 Nanosheets. As mentioned previously, exfoliation, osmotic swelling, and intercalation took place simultaneously in a TBA^+/H^+ range of 5−25. The intercalation phase and osmotically swollen hydrate are composed of multiple MnO_2 sheets. The individual exfoliated nanosheets are therefore expected to be separable from the particles of intercalation compounds and the osmotically swollen manganese oxide by an appropriate centrifugation procedure. We tried to isolate the nanosheets from the sample with $TBA^+/H^+ = 10$, which is composed of the intercalation phase and the exfoliated material. Centrifugation at slower than 6000 rpm separated the intercalation phase as a sediment (Figure 7a). Once the intercalation phase was removed by this procedure, the sediment recovered in further centrifugation at a higher speed had a colloidal appearance and displayed a broad diffraction pattern up to $2\theta = 30°$ (Figure 7b). A similar broad hump has been observed for $Ti_{1-\delta}O_2$ nanosheets derived from a layered titanate via delamination.[5c] The profile is similar to the square of the structure factor, which is calculated as follows based on the structure of the coplanar host layer comprising edge-shared octahedra where Mn and O atoms are located at $z = 0, \pm 0.12$ nm (Figure 6).

$$F(\theta) = f_{Mn} + 2f_O \cos 2\pi[2(0.12)\sin\theta/\lambda] \qquad (1)$$

where f_{Mn} and f_O are the atomic scattering factors for Mn and O atoms.[30] Only the cosine parts are considered because the

(30) *International Tables for X-ray Crystallography*; The International Union of Crystallography; The Kynoch Press: Birmingham, U.K., 1968; pp 201−207.

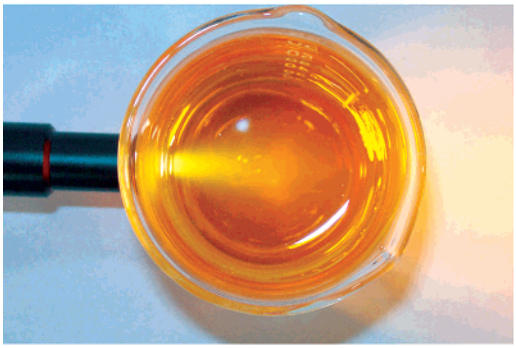

Figure 8. Photograph of a colloidal suspension of MnO_2 nanosheets. The light beam is incident from the side to demonstrate the Tyndall effect. The MnO_2 content was 0.012 g dm^{-3}.[35]

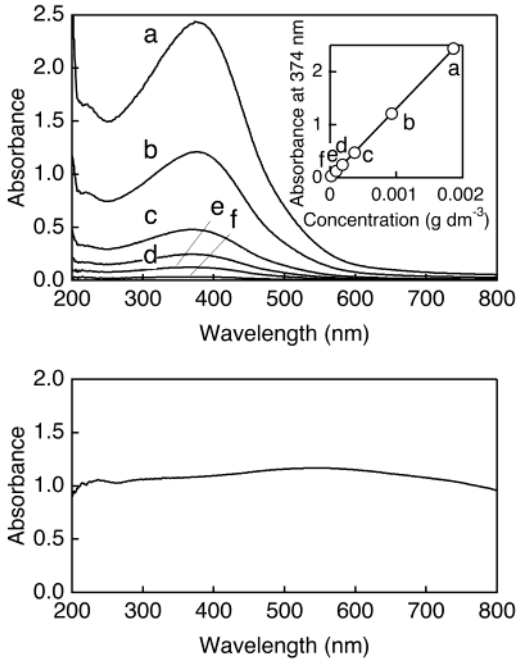

Figure 9. (Top) UV−visible spectra for colloidal suspensions at various concentrations of MnO_2 nanosheets: (a) 1.86×10^{-2} g dm^{-3}, (b) 9.30×10^{-3} g dm^{-3}, (c) 3.72×10^{-3} g dm^{-3}, (d) 1.86×10^{-3} g dm^{-3}, (e) 9.30×10^{-4} g dm^{-3}, (f) 1.86×10^{-4} g dm^{-3}. (Inset) The absorbance at 374 nm is plotted against the nanosheet concentration. (Bottom) A diffuse scattering spectrum for $H_{0.13}MnO_2 \cdot 0.7H_2O$.

nanosheet is centrosymmetric on projection to the *z*-axis. The close match between the observed and calculated data strongly suggests that the pattern can be understood in terms of scattering from the individual MnO_2 sheets with negligible phase interference. Consequently, the broad profile can be taken as evidence of exfoliation of the layered manganese oxide into single layers.

Characterizations of MnO_2 Nanosheets. The colloidal suspension obtained by the procedures previously mentioned was light- to dark-brown, depending on the MnO_2 content. Tyndall light scattering was observed, as shown in Figure 8. The MnO_2 nanosheet crystallites dispersed in the aqueous suspension should be responsible for this phenomenon.

The MnO_2 nanosheets exhibited optical absorption with a broad peak centered around 374 nm (Figure 9, top). Gao et al. have reported similar optical properties for "nanosized birnessite".[22b] This spectral feature differs remarkably from that of the parent layered manganese oxide, $H_{0.13}MnO_2 \cdot 0.7H_2O$. Its diffuse reflectance spectrum revealed an almost constant and

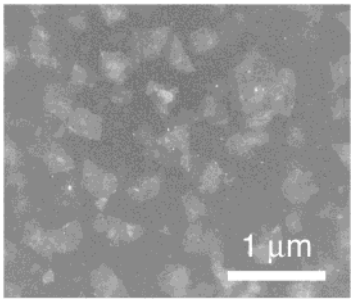

Figure 10. TEM image of MnO_2 nanosheets.

featureless absorption over a wavelength range of 200−800 nm (Figure 9, bottom). Although the different detection mode used to obtain the data makes simple and quantitative comparison difficult, the spectral change upon exfoliation is remarkable and may be associated with the disassemblage of bulk crystals into nanosheets with a sub-nanometer thickness. The absorbance was observed to be linearly dependent on the MnO_2 content (inset of Figure 9, top), excluding a possible association of nanosheets in this concentration range. The molar extinction coefficient, ϵ, at the peak maxima (374 nm) was 1.13×10^4 mol^{-1} dm^3 cm^{-1}.

The morphology of the MnO_2 nanosheets was examined by transmission electron microscopy (TEM) and atomic force microscopy (AFM). A typical TEM image (Figure 10) revealed faint contrasts of dimension less than 1 μm, which is comparable to the crystal dimensions of $H_{0.13}MnO_2 \cdot 0.7H_2O$. The submicrometer to micrometer-sized nanosheets in this study are contrasting to the "nanosized manganese oxide" with lateral dimensions below 50 nm that has been derived by delamination of birnessite.[22b] The image contrast was variable in individual crystallites, which is different from TEM data for other nanosheet crystallites.[6c,7,17b,d,31] They exhibit uniform and homogeneous contrast, reflecting their ultrathin nature and unit thickness. The variation in contrast observed for the MnO_2 nanosheet may be a consequence of its wrinkling or folding, which may occur more easily for the MnO_2 nanosheet compared to thicker nanosheets of $Ti_{1-\delta}O_2$ and $Ca_2Nb_3O_{10}$. The sample did not exhibit sharp electron diffraction spots but provided only a broad halo pattern. This does not necessarily indicate that the nanosheet is amorphous, that is, loss of hexagonal atomic arrangement. Rather, the results suggest a beam-sensitive nature for the extremely thin nanosheets. The XRD data of the restacked product (deposited as Supporting Information) revealed intrasheet reflections at $2\theta = 36°$ and 65°, which are indexable as 10 and 11 for a hexagonal two-dimensional unit cell with $a = 0.30$ nm. This indicates that the two-dimensional crystalline order of the nanosheet remained unchanged during delamination and subsequent restacking.

A tapping-mode AFM image (Figure 11) of the sample adsorbed onto a positively charged surface revealed two-dimensional objects with similar lateral dimensions as those detected by TEM observations, although fragments were also observed in small amounts. The height profile scan indicated that the terrace of the flaky crystallites was fairly flat. The thickness of the nanosheet was measured at steps between the nanosheet and the substrate surface and between the nanosheet and an overlapping nanosheet, yielding average values and standard deviations of 0.91 ± 0.07 and 0.77 ± 0.05 nm,

(31) Sasaki, T.; Watanabe, M. *J. Phys. Chem. B* **1997**, *101*, 10159−10161.

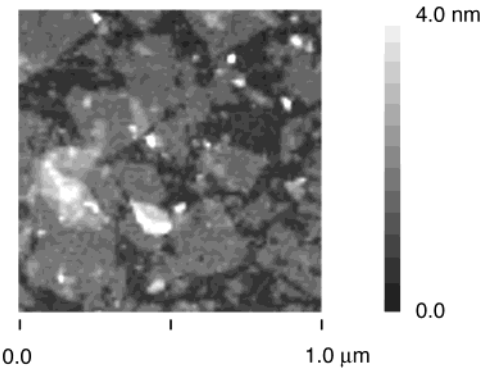

Figure 11. Tapping-mode AFM image of MnO_2 nanosheets.

respectively. The latter results may be more reliable, taking into account the different atomic forces between materials. The highly consistent thickness, a small standard deviation, and its dimension below 1 nm clearly demonstrate the nanosheet nature of the sample. The crystallographic thickness of the nanosheet is evaluated to be 0.52 nm,[29] being based on its atomic architecture (see Figure 6). Hydration of the nanosheets may be responsible for the discrepancy between this thickness and the experimentally obtained value. Similar hydration has been suggested for $Ti_{1-\delta}O_2$ nanosheets.[32]

Restacking Behavior of MnO_2 Nanosheets. The colloidal MnO_2 nanosheets underwent restacking upon drying. Analysis of the restacking process provides important information on the chemical properties of this system. Figure 12 shows XRD data for a colloidal aggregate of MnO_2 nanosheets after centrifugation from suspension and aging in a chamber with a regulated relative humidity of 95%. Aging in this way allows the sample to dry very slowly. The broad profile due to the exfoliated MnO_2 nanosheets was the major feature at an early stage of aging. Also, two different basal diffraction series emerged immediately after the initiation of aging. One indicated a very large spacing of ~10 nm, and the other denoted a relatively small spacing of 1.72 nm. The former can be explained by the aggregation of individual nanosheets to produce an osmotically swollen hydrate, which may be promoted by partial drying of the colloid. We have reported similar behavior for $Ti_{1-\delta}O_2$ nanosheets.[5a] This reaggregation proceeded with time, and the inter-nanosheet separation shrank gradually to ~2.7 nm. This phase did not change further as far as it was in contact with highly moist air (relative humidity at 95%).

The 1.72 nm phase indicates that the nanosheets were also restacked by another route to directly yield a TBA intercalated compound. No change in interlayer distance was observed during the aging process, but the peak intensity increased markedly, indicating an increase in abundance of this structure. Correspondingly, the line width of the basal reflections decreased rapidly with time, suggesting an increase in the number of stacked nanosheets, that is, crystal growth of the intercalation compound. The final product after aging for 24 h was a mixture of the 1.72 and 2.7 nm phases, the former being predominant. The disappearance of the initial broad pattern indicates that all the exfoliated nanosheets had been restacked to give these two phases. The 2.7 nm phase did not survive when the humidity was lowered to 70%, and the 1.72 nm phase persisted as the single discernible phase was at this humidity and below. Further interlayer shrinkage to 1.3 nm was observed only by annealing the sample at 150 °C.

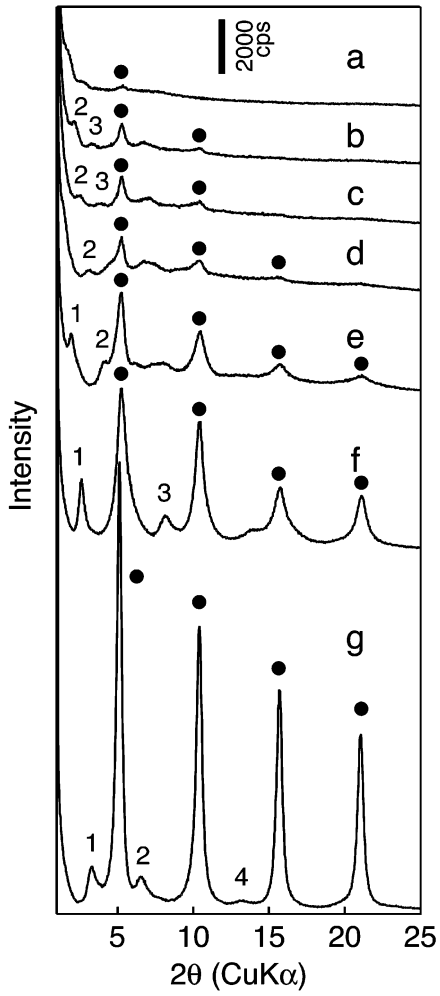

Figure 12. Evolution of XRD profile starting from the colloidal aggregate of MnO_2 nanosheets: (a) start of aging, (b) after 2.3 h, (c) 4.7 h, (d) 7.0 h, (e) 9.3 h, (f) 11.7 h, and (g) 23.3 h. Circles designate the basal diffraction series for the TBA intercalated phase ($d = 1.72$ nm). The numerals represent the orders of basal reflections of the osmotically swollen phase. Intersheet separations are (b) 7.2 nm, (c) 6.1 nm, (d) 5.5 nm, (e) 4.5 nm, (f) 3.4 nm, and (g) 2.7 nm.

The structural considerations for the 1.25 nm phase formed in the TBA intercalation process to $H_{0.13}MnO_2 \cdot 0.7H_2O$ indicate that TBA ions are accommodated as a monolayer in the manganese oxide gallery (Figure 6). The 1.72 nm phase may be accounted for by the insertion of additional H_2O layers. Interestingly, the intercalation compounds with different hydration states were formed in the forward intercalation process and in the restacking reaction.

There have been a few reports on the intercalation of TBA ions into birnessite, one of the layered manganese oxides. Liu et al. reported that birnessite did not take up TBA ions directly.[22a] Their incorporation was only attained by pre-intercalation of smaller tetramethylammonium (TMA) ions and subsequent replacement with TBA ions. The product accommodated TMA as well as TBA ions with two layers of H_2O molecules in the gallery, which had a separation of 2.19 nm in the wet state. In contrast, Gao et al. reported the direct formation of a 1.69 nm phase through the action of aqueous TBA ions,

(32) Sasaki, T.; Ebina, Y.; Kitami, Y.; Watanabe, M.; Oikawa, T. *J. Phys. Chem. B* **2001**, *105*, 6116−6121.

although the corresponding broad XRD pattern suggests the poor crystalline nature.[22b] This intersheet spacing was explained by accommodation of TBA ions with one layer of H_2O molecules. These structures were stable only in a wet state and collapsed upon drying. The 2.19 nm phase reported by Liu et al. was disproportionated into three poorly crystalline phases having interlayer distances of 0.96, 1.25, and 1.99 nm.[22a] Strangely, air-drying of the 1.69 nm phase squeezed TBA ions from the interlayer space.[22b] These results suggest that the intercalation behavior of birnessite and the stability of the evolved phases vary significantly between samples.

Birnessite including samples employed in the studies mentioned previously has been synthesized mostly via solution-phase reactions under ambient conditions by oxidation of Mn^{2+} or reduction of MnO_4^- or redox between these two species. Generally, synthesis at low temperatures does not yield a sample with a large crystallite size. The chemical reactivity of such samples may therefore vary. The protonic manganese oxide in this study has structural and compositional features comparable to those of birnessite but may be contrasting to those of the "birnessite", prepared so far in solution, in terms of its micrometer-sized crystallites, well-developed platelike shape (see Figure 1), and high crystallinity, because its starting material $K_{0.45}MnO_2$ was prepared in solid-state calcination at high temperature. These features may lead to well-defined swelling and delamination behavior and nanosheets with large lateral dimensions.

Conclusions

Upon contact with aqueous TBA ions, the layered manganese oxide $H_{0.13}MnO_2 \cdot 0.7H_2O$ underwent various reactions including intercalation, osmotic swelling, and delamination into single sheets, which was dependent on the TBA concentration. Separation from other coexisting phases via centrifugation successfully isolated unilamellar crystallites of MnO_2, which are only 0.77 nm in thickness and several hundreds nanometers in lateral size. Slow drying of these colloidal nanosheets proceeded via two different routes, producing the TBA intercalated phase and the osmotically swollen hydrate.

Experimental Section

Reagents and Materials. The layered manganese oxide $K_{0.45}MnO_2$ was prepared by calcining a stoichiometric mixture of KOH and Mn_2O_3 at 1073 K for 60 h under O_2 gas flow.[23] The obtained compound (~10 g) was treated with 2 dm^3 of HCl solution (1 mol dm^{-3}). The acid solution was replaced with a new one every 24 h. Repetition of this acid-digestion procedure for 10 days achieved nearly complete removal of interlayer K ions. The resulting solid, $H_{0.13}MnO_2 \cdot 0.7H_2O$, was washed with copious amounts of water and then air-dried. The chemicals used were of reagent grade or higher purity. Milli-Q filtered water was used throughout the experiments.

Equilibrations. A weighed amount (0.4 g) of $H_{0.13}MnO_2 \cdot 0.7H_2O$ was equilibrated with 100 cm^3 of an aqueous TBAOH solution for at least 10 days at 298 ± 0.5 K. The dose of TBAOH applied with respect to the amount of exchangeable protons in $H_{0.13}MnO_2 \cdot 0.7H_2O$, that is, a molar ratio of TBA^+/H^+, was varied between 0.1 and 100 by changing the concentration of TBA hydroxide.

Chemical Analysis. K and Mn contents were determined by inductively coupled plasma atomic emission spectroscopy (ICP-AES; Seiko HRV-1700 spectrophotometer) after dissolving a sample (~50 mg) with a solution of $HNO_3 + H_2O_2$. The H_2O content was estimated from the weight loss by heating to 1000 °C, taking the oxygen release due to reduction to trivalent Mn into account. Carbon and nitrogen contents in TBA intercalated compounds were determined using a Perkin−Elmer 2400 CHNS/O analyzer.

The mean valency of Mn was obtained by standard titration with oxalic acid.[33] A weighed amount of sample (~80 mg) was dissolved by heating in a mixed solution of COONa and H_2SO_4. Excess COONa was determined by titration with standard $KMnO_4$ solution.

Instrumentation. A powder X-ray diffractometer (Rigaku Rint-2000S) with graphite-monochromatized Cu Kα radiation ($\lambda = 0.154\,05$ nm) was employed to collect XRD data for aqueous samples obtained by equilibration as previosly mentioned and for solid samples centrifuged therefrom. The relative humidity in the sample chamber was regulated at 95% to suppress undesirable drying of the fluid or colloidal samples, unless mentioned otherwise.

UV−visible absorption spectra were measured in a transmission mode using a Hitachi U-4000 spectrophotometer.

TEM observations were performed using a JEOL 1010 electron microscope operating at an accelerating voltage of 100 kV. A drop of the diluted suspension was placed onto a carbon-coated Cu grid and removed after a certain period (~5 min). The obtained TEM grid was allowed to be observed.

Scanning electron micrographs (SEM) were obtained using a Hitachi H-5000 electron microscope (accelerating voltage at 10 kV). Samples were coated with ~4 nm of Os metal to suppress charging.

A Seiko SPS-1100 AFM instrument was employed to obtain a topographical image of the nanosheets. Samples were prepared by adsorbing the nanosheets from suspension onto a mica substrate precoated with a cationic polymer, polyethylenimine. Measurements were carried out in tapping mode with an Si cantilever having a force constant of 20 N m^{-1}.

Acknowledgment. The authors are grateful to Mr. K. Kurashima of the National Institute for Materials Science for assistance with TEM observations.

Note Added after ASAP Publication: The version published on the Web 3/1/2003 contained errors in the references. The final Web version published 3/7/2003 and the print version are correct.

Supporting Information Available: XRD data for a TBA intercalated compound obtained by freeze-drying a colloidal suspension of the MnO_2 nanosheets (1 page). Basal 00*l* reflections indicate an intersheet distance of 1.72 nm. The 10 and 01 peaks arise from the two-dimensional periodicities in the MnO_2 sheets. Random stacking of the sheets is responsible for the observed asymmetric profile. This material is available free of charge via the Internet at http://pubs.acs.org.

JA021364P

(33) JIS M8233. *Methods for Determination of Active Oxygen in Manganese Ores*; Japanese Industrial Standards Committee, 1969.
(34) Shannon, R. D. *Acta Crystallogr.* **1976**, *A32*, 751−767.
(35) The nanosheet content of the suspension was determined gravimetrically by drying 10 cm^3 of the sample and heating at 1000 °C. The calcined residue was weighed as Mn_2O_3.